

# Simultaneous Multicolor Observations of Starlink’s Darksat by The Murikabushi Telescope with *MITSuME*

TAKASHI HORIUCHI,<sup>1</sup> HIDEKAZU HANAYAMA,<sup>1</sup> AND MASATOSHI OHISHI<sup>2,3</sup>

<sup>1</sup>*Ishigakijima Astronomical Observatory,  
Public Relations Center,*

*National Astronomical Observatory of Japan,  
1024-1 Arakawa, Ishigaki, Okinawa, 907-0024, Japan*

<sup>2</sup>*Spectrum Management Office, Public Relations Center,  
National Astronomical Observatory of Japan,  
2-21-1 Osawa Mitaka Tokyo 181-8588, Japan*

<sup>3</sup>*Department of Astronomical Science,  
SOKENDAI (The Graduate University for Advanced Studies),  
2-21-1 Osawa, Mitaka, Tokyo 181-8588, Japan*

(Received October 9, 2020; Accepted March 17, 2024)

## ABSTRACT

We present the SDSS  $g'$ -, the Cousins  $R_c$ -, and  $I_c$ -band magnitudes and associated colors of the Starlink’s STARLINK-1113 (one of the standard Starlink satellites) and 1130 (Darksat) with a darkening treatment to its surface. By the 105 cm Murikabushi telescope/*MITSuME*, simultaneous multicolor observations for the above satellites were conducted four times: on April 10, 2020, May 18, 2020 (for Darksat), and June 11, 2020 (for Darksat and STARLINK-1113). We found that (1) the SDSS  $g'$ -band apparent magnitudes of Darksat ( $6.95 \pm 0.11 - 7.65 \pm 0.11$  mag) are comparable to or brighter than that of STARLINK-1113 ( $7.69 \pm 0.16$  mag), (2) the shorter the observed wavelength is, the fainter the satellite magnitudes tend to become, (3) the reflected flux by STARLINK-1113 is extremely ( $> 1.0$  mag) redder than that of Darksat, (4) there is no clear correlation between the solar phase angle and orbital-altitude-scaled magnitude, (5) by flux-model fitting of the satellite trails with the blackbody radiation, it is found that the albedo of Darksat is about a half of that of STARLINK-1113. Especially, the result (1) is inconsistent with the previous studies. However, considering both solar and observer phase angles and atmospheric extinction, the brightness of STARLINK-1113 can be drastically reduced in the SDSS  $g'$  and the Cousins  $R_c$  band. Simultaneous multicolor-multispot observations more than three colors would give us more detailed information regarding the impact by the low Earth orbit satellite constellations.

**Keywords:** astronomical research — astronomical site protection — observatories

## 1. INTRODUCTION

SpaceX launched 60 Starlink satellites to low Earth orbit (LEO) on May 24, 2019 as the first batch of a large constellation. Furthermore, SpaceX plans to launch 42,000 Starlink LEO communication satellites in total until Mid 2020s. On June 3, 2019, the International Astronomical Union (IAU) expressed its concern on the fact that the extremely bright magnitude of these communication satellites affect astronomical observations and the pristine appearance of the night sky<sup>1</sup>.

In response to the concern by the IAU, SpaceX has tried to reduce satellite brightness, and has also asked astronomers to measure the satellite brightness. After the launch of the Starlink satellites, their apparent magnitude and impact on astronomical observations were reported by previous studies using ground-based telescopes. Hainaut & Williams (2020) investigated the impact by mega-constellations of the LEO satellites in the optical and IR wavelength regions on the ESO telescopes. They concluded that very wide-field imaging surveys will be terribly ruined due to saturation and/or ghosting by a satellite. McDowell (2020) also concluded that certain types of observation such as long-exposure

<sup>1</sup> <https://www.iau.org/news/pressreleases/detail/iau2001/>

and twilight observations with wide fields of view (FoV) will be significantly affected by the Starlink satellites.

SpaceX launched the third batch of the 60 LEO satellites on January 7, 2020. One of the 60 satellites is the prototype satellite, STARLINK-1130 (nicknamed Darksat) where the communication antenna is coated with painting to reduce reflected sunlight to the Earth (see Figure 7 of Tyson et al. 2020). As the first observational attempt, Tregloan-Reed et al. (2020; hereafter, Tr20) estimated the Sloan  $g'$  magnitude of Darksat and STARLINK-1113 and suggested that Darksat is  $0.77 \pm 0.05$  magnitude fainter than STARLINK-1113. However, simultaneous multicolor observations for these satellites have not been reported yet despite the importance of this kind of observation. The simultaneity of the observations ensures the same conditions in multiple bands: same coordinate, airmass, and exposure time, and so on. Not only that, it is able to examine the darkening effects of satellite-surface by the color estimation and/or radiation model fitting for these LEO communication satellites under the simultaneous multicolor observations.

In this paper, we report the multi-band (the SDSS  $g'$ , the Cousins  $R_c$ , and  $I_c$ ; hereafter  $g'$ ,  $R_c$ , and  $I_c$  for simplicity) magnitudes and colors of Darksat and STARLINK-1113 with simultaneous multicolor observations using the 1.05m Murikabushi telescope/*MITSuME* system. In Section 2, the observations and the data analysis for Darksat and STARLINK-1113 are presented. We show the apparent and orbital-altitude-scaled magnitudes of the satellites in Section 3. In Section 4, we discuss (1) the effects of atmospheric extinction to the satellites, and (2) modeling the AB flux of the satellites.

## 2. OBSERVATIONS AND DATA ANALYSIS

### 2.1. Observations

Ishigakijima Astronomical Observatory (IAO) of the National Astronomical Observatory of Japan operates the 105 cm Murikabushi telescope (F12) with *MITSuME*<sup>2</sup>. The *MITSuME* system equipped with the Murikabushi telescope has three CCD cameras (Apogee Alta U-6) with  $1024 \times 1024$  pixels, and enables us simultaneous  $g'$  (477 nm)-,  $R_c$  (649.2 nm)- and  $I_c$  (802 nm)-band observations, where the values in the parenthesis indicate the effective wavelengths in each band. Among the three bands  $R_c$  band has the most highest sensitivity. The F-value of the Murikabushi telescope is adjusted from F12 to F6.5 via the conversion lenses in

the *MITSuME* system; it yields a FoV of  $12.3 \times 12.3$  arcmin<sup>2</sup> and a pixel scale of 0.72 arcsec pixel<sup>-1</sup>.

Based on the two-line element (TLE) data from the satellite catalog of the Celestrak website<sup>3</sup> and the forecast time and equatorial coordinates extracted from Heavensat<sup>4</sup>, we carried out simultaneous multicolor observations for the light trail of Darksat and STARLINK-1113 using the Murikabushi telescope/*MITSuME* between April and June, 2020. Table 1 lists the observation log in this study. Since the satellites move so fast, we were not able to track them. Instead we pointed the telescope to the calculated position of a satellite, and waited for the satellite passing by the field of view.

The observed flux of satellites,  $f_{\text{sat}}$ , is inversely proportional to angular velocity of the satellite along the celestial sphere,  $V_{\text{sat}}$ , therefore, the apparent magnitude of satellites,  $m_{\text{sat}}$ , is written as follows:

$$m_{\text{sat}} = m_{\text{star}} - 2.5 \log \left( \frac{V_{\text{sat}}}{V_{\text{star}}} \frac{f_{\text{sat}}}{f_{\text{star}}} \right), \quad (1)$$

where  $V_{\text{star}}$ ,  $f_{\text{star}}$ , and  $m_{\text{star}}$  are the angular velocity along the celestial sphere, flux, and magnitude of reference stars (i.e.,  $V_{\text{star}} = 15 \times \cos \delta$  arcsec s<sup>-1</sup>,  $\delta$ : declination), respectively. Here, we observed the satellites with star tracking, and after that, the reference stars were observed by stopping the star tracking immediately. The velocity of the reference stars during fixed observation is  $V_{\text{star}}$ . It is possible to estimate the angular velocity,  $V_{\text{sat}}$ , by calculating a traverse speed on the great-circular distance,  $\lambda$ , which is written as follows:

$$\lambda = \arccos(\sin \delta \sin D + \cos \delta \cos D \cos(A - \alpha)), \quad (2)$$

where  $(\alpha, \delta)$  and  $(A, D)$  are the right ascension, declination of satellites at the initial time of an observation and those at a certain time, respectively. In order to measure the flux of reference stars,  $f_{\text{star}}$ , by the same way to evaluate flux of satellite trails, we elongated the CCD images of reference stars so that the images become the same shape as satellite light trails. Figures 1, 2, 3, and 4 show the FITS images of Darksat and elongated reference stars around the satellite trail. In Figures 1 and 4, we do not include the bright stars on a right-side edge of images for reference stars due to a count bias on the CCD image of the  $I_c$  band. Since there are no bright reference stars without the count bias around the STARLINK-1113 trail (Figure 4), we added and observed a bright reference star near the target field (i.e.,

<sup>2</sup> This is an abbreviation of Multi-color Imaging Telescopes for Surveys and Monstrous Explosions. It means “three eyes” in Japanese.

<sup>3</sup> <https://celestrak.com/satcat/search.php>

<sup>4</sup> <http://www.sat.belastro.net/heavensat.ru/english/index.html>

three reference stars for the STARLINK-1113 trail, see Table 2).

### 2.2. Data Analysis

We performed dark subtraction, dome flat corrections and sky subtraction with Image Reduction and Analysis Facility (IRAF). In the actual data analysis, we subtracted bad pixels and stars from the original satellite trail images (see middle panels of Figures 1, 2, 3, and 4). In this study we adopted the star catalog UCAC4 that is, for instance, able to refer to Johnson’s  $B$ ,  $V$ , SDSS  $r$ , and  $i$  band magnitudes. It is possible to derive  $g'$ -,  $R_c$ - and  $I_c$ -band magnitudes using the equations in Table 3 of Jordi et al. (2006):

$$g = V + 0.630(B - V) - 0.124, \quad (3)$$

$$R = r - 0.252(r - i) - 0.152, \quad (4)$$

$$I = r - 1.245(r - i) - 0.387. \quad (5)$$

We measured the count profile perpendicular to the streak for each object, and compared the corresponding profile from the elongated star image. We note again that the flux per unit length of the streak is inversely proportional to the angular velocity of an object (see Equation (1)). We used *Projection* in SAOImage DS9<sup>5</sup> to measure the flux (averaged counts of cross sections) in a rectangular-region for the integration along the Darksat and STARLINK-1113 trails, and the reference stars around these satellite trails. The rectangular region to measure the averaged satellite flux,  $f_{\text{sat}}$ , is 10 times thicker than that of the reference stars but avoiding the edge of CCDs (i.e., the trail length was limited in measuring its flux), and then we integrated the area under the profile. Figure 5 exhibits averaged CCD counts along the Darksat and STARLINK-1113 trails.

The statistical magnitude errors,  $\sigma_m$ , of Darksat and STARLINK-1113 were estimated by applying the law of error propagation to Equation (1):

$$\sigma_m = \frac{2.5}{\ln 10} \sqrt{\left(\frac{\delta f_{\text{sat}}}{f_{\text{sat}}}\right)^2 + \left(\frac{\delta f_{\text{star}}}{f_{\text{star}}}\right)^2 + \left(\frac{\delta V_{\text{sat}}}{V_{\text{sat}}}\right)^2}, \quad (6)$$

where  $\delta f_{\text{sat}}$ ,  $\delta f_{\text{star}}$ , and  $\delta V_{\text{sat}}$  are the flux errors of light trails of satellites and reference stars, and the velocity error of satellites, respectively. In this study, these errors take the following ranges:  $0.005 \lesssim \delta f_{\text{sat}}/f_{\text{sat}} \lesssim 0.07$ ,  $0.004 \lesssim \delta f_{\text{star}}/f_{\text{star}} \lesssim 0.21$ , and  $0.002 \lesssim \delta V_{\text{sat}}/V_{\text{sat}} \lesssim 0.06$ . Since the angular velocity of the reference stars,  $V_{\text{star}}$ , is constant, we ignored in Equation (6) the term related with the angular velocity of

stars. We estimated the standard deviation of sky flux,  $\sigma_{\text{sky}}$ , around the satellite trails to evaluate the flux errors of the trails,  $\delta f_{\text{sat}}$ , and those of reference stars,  $\delta f_{\text{star}}$ . Here, the sky region to estimate  $\sigma_{\text{sky}}$  has the same rectangular shape when we estimated the flux of trails by satellites or reference stars (i.e.,  $\delta f_{\text{sat}}$  or  $\delta f_{\text{star}} = \sigma_{\text{sky}} \times \text{pixel width of trails}$ ). The velocity error of satellites,  $\delta V_{\text{sat}}$ , is an averaged value of the velocity difference between the central to start exposure time,  $|V_{\text{sat}} - V_{\text{start}}|$ , and that of the central to end time,  $|V_{\text{sat}} - V_{\text{end}}|$ .

## 3. RESULTS

In this section, we provide the multi-band magnitudes and colors of the Darksat and STARLINK-1113 trails.

### 3.1. Apparent and Normalized Magnitude

First, we measured the apparent magnitudes of Darksat and STARLINK-1113 as described in the previous section. In addition to correcting the difference of the distance between an observer and a satellite, we normalized these magnitudes at the satellite orbital altitude of  $\sim 550$  km (hereafter, normalized magnitude) by adding a factor of  $+5\log(r/550)$ , where  $r$  is the distance between the satellite and observer (see also Tr20 and Tyson et al. 2020). We considered the errors of  $r$  for the estimation of the normalized magnitudes. Table 2 summarizes the reference stars, apparent, and normalized  $g'$ -,  $R_c$ -, and  $I_c$ -band magnitudes for each observation epoch. The apparent and normalized  $g'$ -band magnitudes of Darksat ( $7.37 \pm 0.10$  and  $6.35 \pm 0.10$  mag on average) are slightly brighter than that of STARLINK-1113 ( $7.69 \pm 0.16$  and  $6.68 \pm 0.17$  mag) in our measurements, while those of Darksat are fainter than STARLINK-1113 in  $R_c$  and  $I_c$  bands. We found a tendency that the longer the observed wavelength is, the brighter the two satellite magnitudes become. Especially, STARLINK-1113 showed the extremely bright  $I_c$ -band magnitude of  $5.25 \pm 0.07$  (apparent magnitude) and  $4.25 \pm 0.07$  mag (normalized magnitude).

Next, we estimated the colors of the Darksat and STARLINK-1113 trails. Under the simultaneous multicolor observations, the largest advantage of color estimations is that the effects on each band can be tested without considering the dependence on the all parameters such as a satellite orbital altitude (or the distance  $r$ ), angular velocity, and solar (or observer) phase angle. Table 3 lists the colors  $g' - R_c$ ,  $g' - I_c$ , and  $R_c - I_c$  of Darksat and STARLINK-1113 in each observation epoch. In the case of Darksat, while there is no significant color difference between May 18 and June 11, that of April 10 is different from the data of the other

<sup>5</sup> <https://sites.google.com/cfa.harvard.edu/saoimageds9>



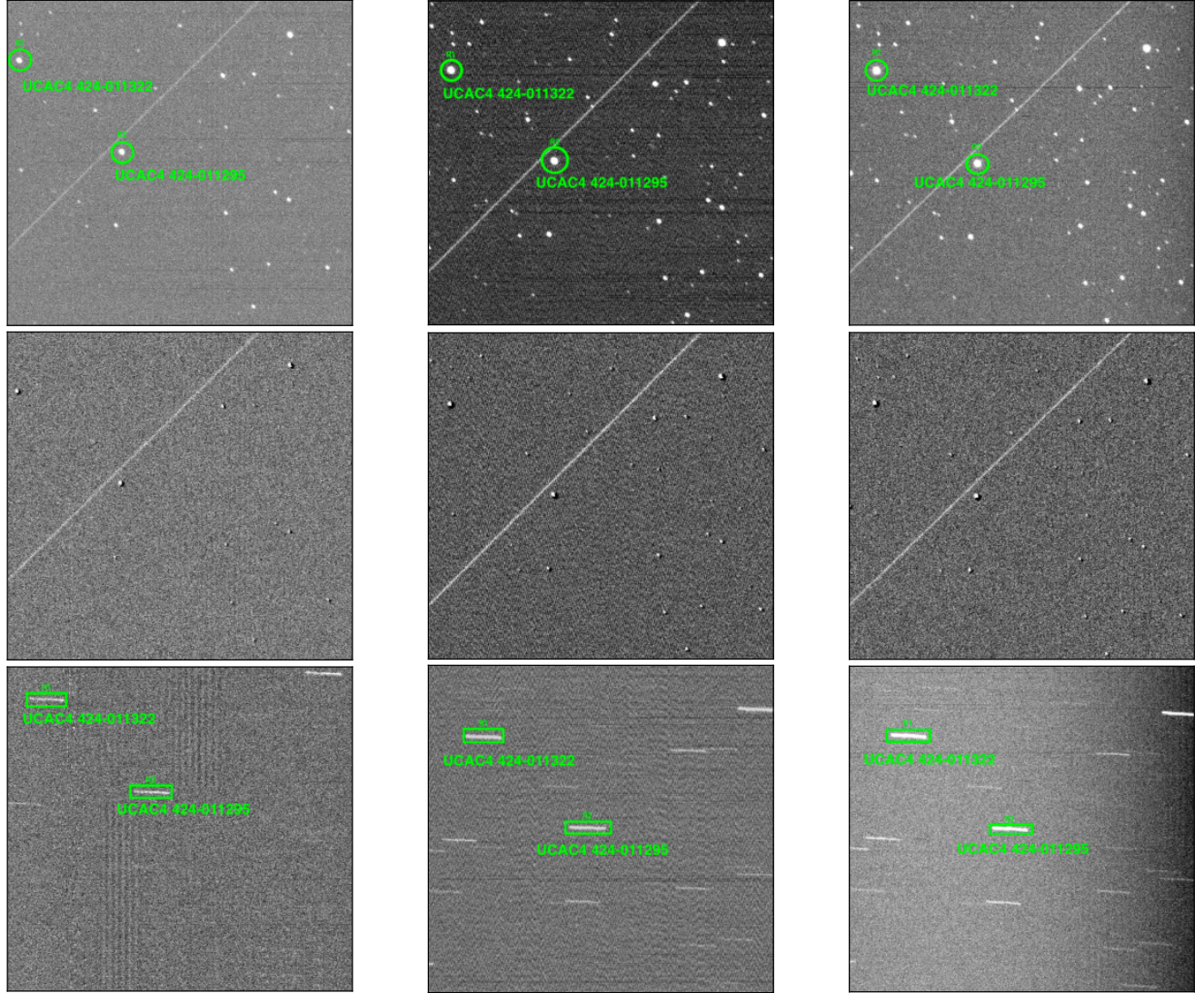


**Figure 1.** The FITS images of Darksat (top), bad-pixel-subtracted images (middle), and elongated reference stars (bottom) in April 10, 2020 taken by the Murikabushi telescope/*MITSuME*  $g'$  (left),  $R_c$  (center), and  $I_c$  (right) bands. Reference stars around the satellite trails are marked with circles (top) or rectangles (bottom).

two epochs due to the weather condition. The colors  $g' - I_c$ , and  $R_c - I_c$  of STARLINK-1113 are extremely ( $> 1$  mag) redder than that of Darksat for any observation epochs.

### 3.2. Phase Angle Effect

We used the orbital information in HORIZONS Web-Interface<sup>6</sup> in order to examine solar phase angle dependence of the normalized magnitudes (see also Table 1). In Figure 6 we plotted our data point on the solar phase angles vs normalized  $g'$ -,  $R_c$ -, and  $I_c$ -band magnitudes

plane together with the results of Tr20. The  $g'$ , and  $R_c$ -band magnitudes of Darksat do not show any clear relation with the solar phase angle. Those of  $g'$  band are consistent with that of Tr20 despite a solar phase angle difference of  $\sim 40^\circ - 55^\circ$ . On the other hand, the  $g'$ -band magnitude of STARLINK-1113 is  $\sim 1.5$  mag darker than that of Tr20 in spite of the smaller one of  $\sim 6^\circ$ . Consequently, the multi-band magnitudes do not exhibit a clear correlation with solar phase angles. The phase angle effect alone cannot explain the magnitude difference between Darksat and STARLINK-1113 (see Appendix A about both the solar and observer phase-angle effects). This may be due to the small number of observation points, and it would be needed to conduct more

<sup>6</sup> <https://ssd.jpl.nasa.gov/horizons.cgi>



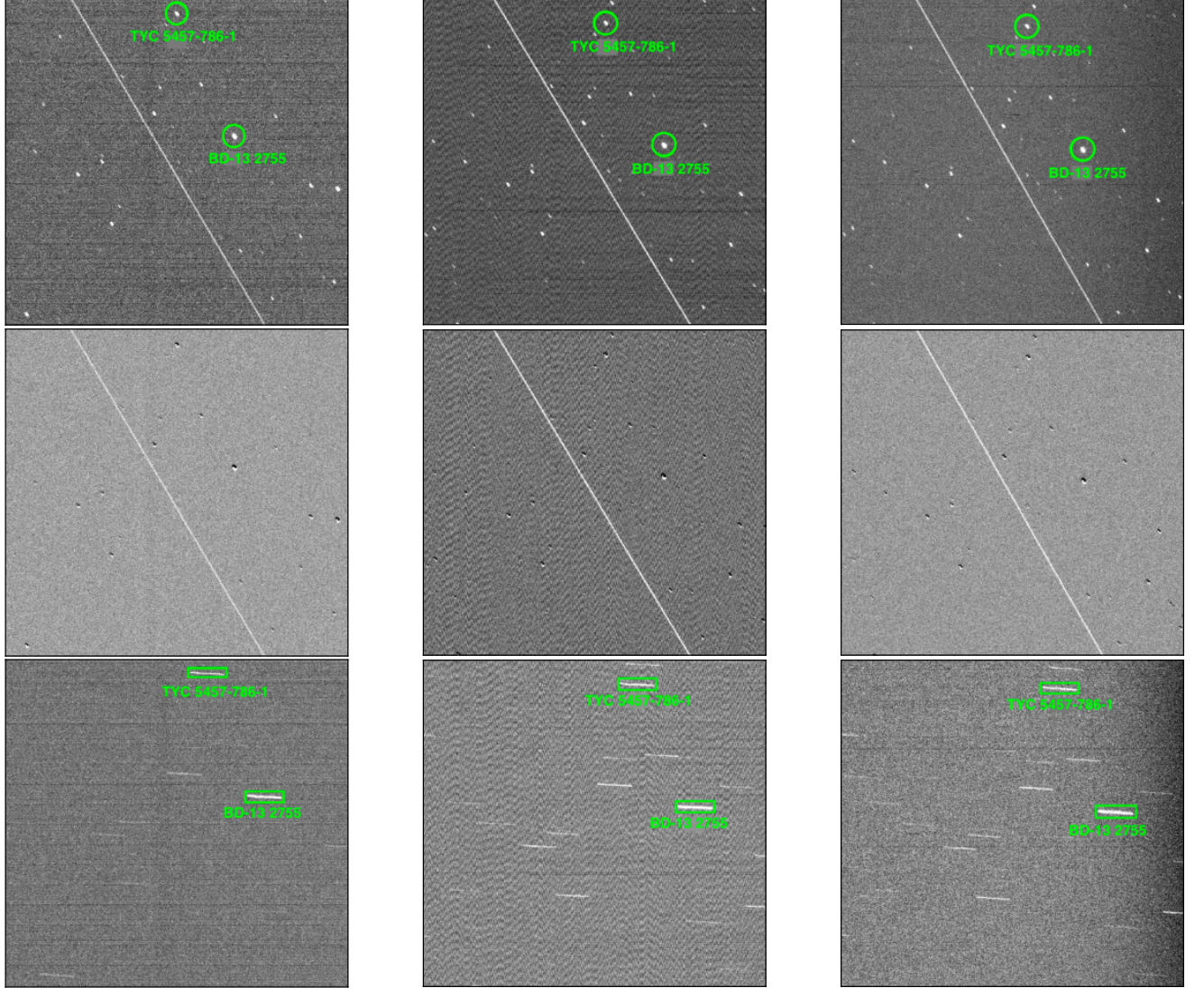


**Figure 2.** Same as Figure 1, but for the Darksat images in May 18, 2020.

frequent observations to reveal if there is a relation between satellite brightness and solar phase angle.

#### 4. DISCUSSION

##### 4.1. The effect of Atmospheric Extinction

The STARLINK-1113 trail showed extremely redder color than the Darksat trail (Table 3). We will discuss below the effect of atmospheric extinction. The STARLINK-1113 trail was observed on June 11, 2020 12:18:00 UTC in this study. Shortly after 12:18:10 UTC, this satellite plunged into the Earth shadow. As shown in Figure 7, we define the following angles: (1) angle,  $\theta_1$ , between the line from the geocenter to ground surface (i.e., the Earth radius  $R_\oplus = 6371$  km) and the line from the geocenter to the satellite orbital altitude at the beginning of the Earth shadow  $l$  of 6921 km (point B), (2)

angle,  $\theta_2$ , between the line from the geocenter to the upper edge of the atmosphere (i.e.,  $R_\oplus + \Delta R$  of 6471 km) and the line from the geocenter to the intersecting point with the tangent line of the upper atmosphere (point A; the same length as  $l$ ). A range of angle,  $\theta_1 - \theta_2$ , where atmospheric extinction becomes noticeable is written as follows:

$$\theta_1 - \theta_2 = \arctan\left(\frac{\sqrt{l^2 - R_\oplus^2}}{R_\oplus}\right) - \arctan\left(\frac{\sqrt{l^2 - (R_\oplus + \Delta R)^2}}{R_\oplus + \Delta R}\right) \sim 2.22 \text{ [deg]}. \quad (7)$$

Since the orbital period of STARLINK-1113 was 95.64 min at the observation time, the angular velocity of



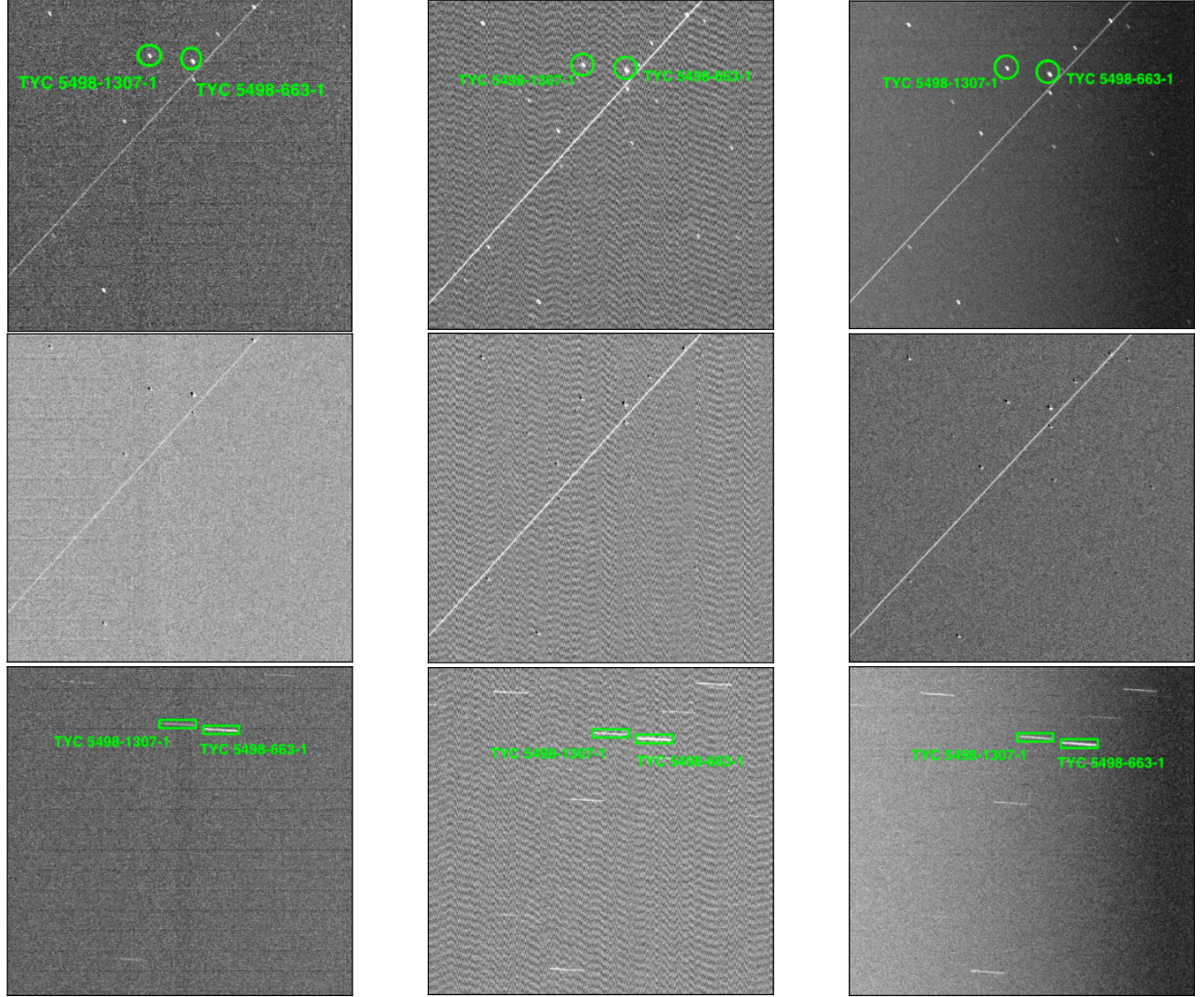


**Figure 3.** Same as Figure 1, but for the Darksat images in June 10, 2020.

STARLINK-1113 was  $\sim 0.06 \text{ deg s}^{-1}$ ; the time required to cross the range,  $\theta_1 - \theta_2$ , is  $\sim 35.4 \text{ s}$ . Namely, STARLINK-1113 was orbiting in the vicinity of the entrance to the Earth shadow at our observation time, and was strongly affected by the atmospheric scattering in the  $g'$ , and  $R_c$  bands. The Earth shine and terrestrial radiation would also contribute magnitudes of satellite trails. However, the contribution of these radiation can be reduced in the Earth shadow. Other than the altitudes and the phase angles of satellite, the effect of atmospheric extinction should also be taken into account as another factor. In other words, the brightness of the usual Starlink's LEO satellites can be reduced comparable to that of Darksat by taking into account the above effects.

#### 4.2. Modeling the Flux of Darksat and STARLINK-1113

##### 4.2.1. Effective Radiation Temperature of Darksat and STARLINK-1113

We evaluate the surface temperature of Darksat and STARLINK-1113 from the apparent magnitudes,  $m_{\text{Sat}}$ , in Table 2. Although these LEO satellites have a shape of flat panel, if we assume the satellites are spherical, the surface temperature,  $T_{\text{sat}}$ , is written as follows (Spencer et al. 1989):

$$T_{\text{sat}} = \left( \frac{I(1 - a_{\text{obs}})}{4\sigma\epsilon} \right)^{\frac{1}{4}}, \quad (8)$$

where  $I$  ( $= 1.37 \times 10^3 \text{ W m}^{-2}$ ),  $a_{\text{obs}}$ ,  $\epsilon$  ( $= 0.9$ ), and  $\sigma$  ( $= 5.67 \times 10^{-8} \text{ W m}^{-2} \text{ K}^{-4}$ ) are the solar constant, mea-



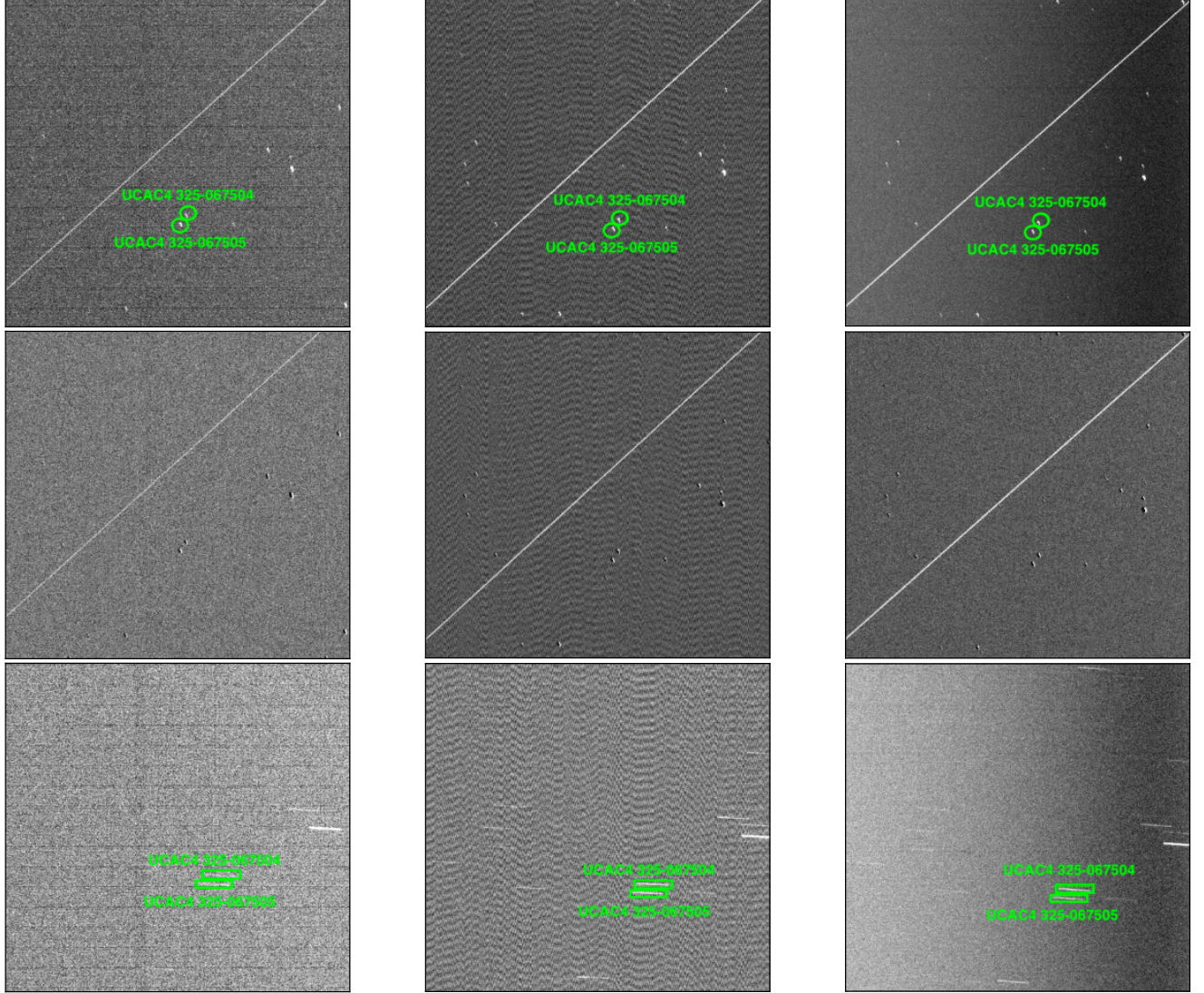


**Figure 4.** Same as Figure 1, but for the STARLINK-1113 images in June 10, 2020.

sured surface albedo, the infrared emissivity (Lebofsky et al. 1986), and the Stefan-Boltzmann constant, respectively. For estimating of the surface temperature,  $T_{\text{sat}}$ , we need to derive the absolute magnitude of these satellites,  $H$ :

$$H = m_{\text{Sun}} - 2.5 \log \frac{a_{\text{obs}} r_{\text{sat}}^2}{(1\text{au})^2}, \quad (9)$$

where  $m_{\text{Sun}}$  and  $r_{\text{sat}}$  are the apparent magnitude of the Sun (Willmer 2018) and the radius of Darksat or STARLINK-1113, respectively. We employed the radius,  $r_{\text{sat}}$ , of 1.5 m for the Starlink satellites (i.e., the flat panel with a diameter of 3 m; McDowell 2020). The  $H$  for the LEO satellites is also approximately described by the phase integral,  $p(\theta)$ , as a first-approximation func-

tion of the solar phase angle  $\theta$  (Whitmell 1907):

$$m_{\text{sat}} \sim H - 2.5 \log \left( \frac{(1 \text{ au})^2 p(\theta)}{r^2} \right), \quad (10)$$

$$p(\theta) = \frac{2}{3} \left( \left( 1 - \frac{\theta}{\pi} \right) \cos \theta + \frac{1}{\pi} \sin \theta \right), \quad (11)$$

where  $r$  is the distance between an observer and a satellite. It is able to derive the surface albedo,  $a_{\text{obs}}$ , from Equations (9) through (11). Then, the surface temperature,  $T_{\text{sat}}$ , is evaluated immediately. Table 4 summarizes the surface temperature of Darksat and STARLINK-1113 in this study. From Table 4, we adopt the temperature,  $T_{\text{sat}}$ , of 280 K to be used in the following discussion. We note the satellite radius of 1.5 m is an approximate value and has an uncertainty,  $\delta r_{\text{sat}}$ .

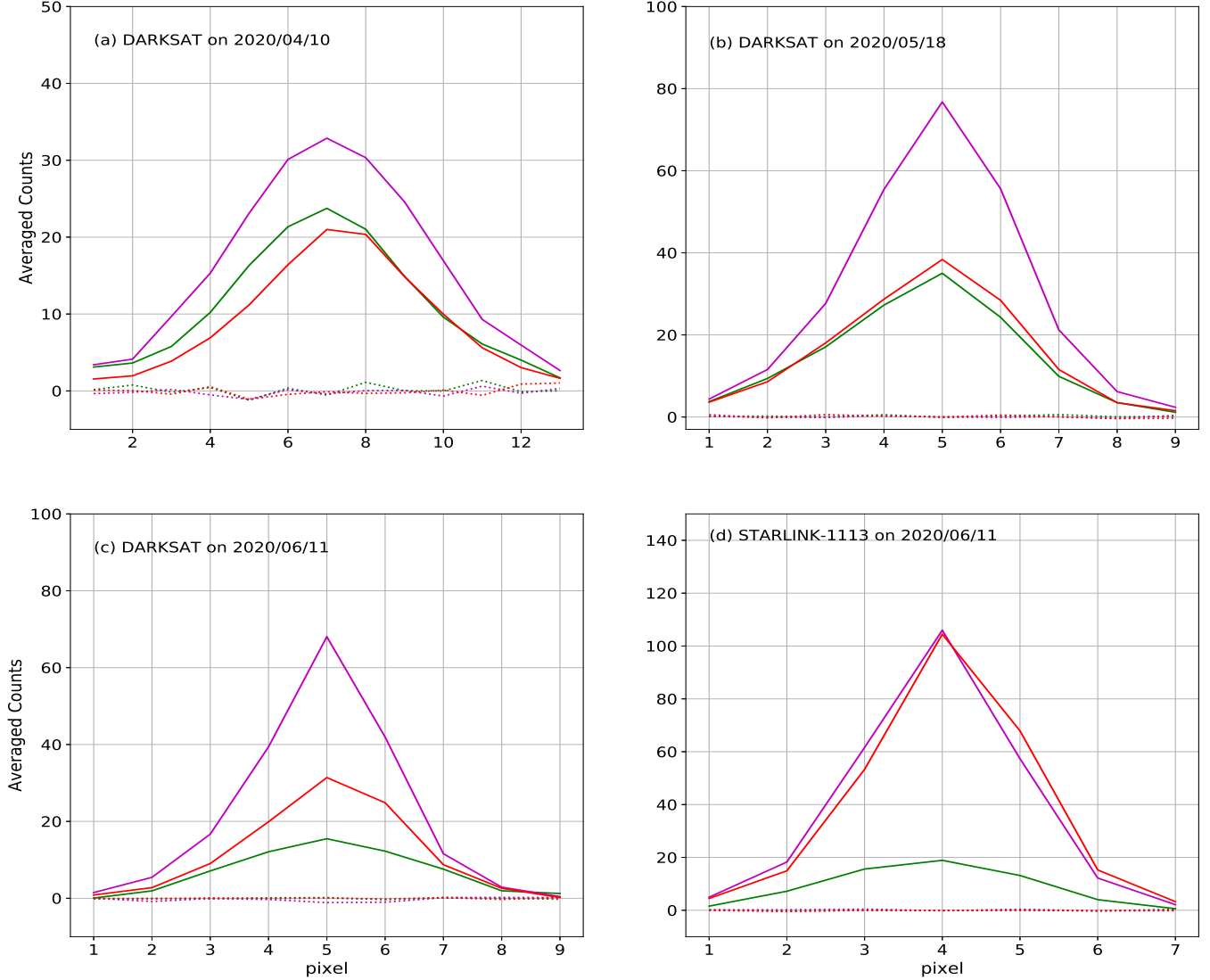


**Figure 5.** Averaged-section counts along the Darksat and STARLINK-1113 trails in the Murikabushi telescope/*MITSuME*  $g'$  (green),  $R_c$  (magenta), and  $I_c$  (red) bands. Solid and dotted lines indicate counts of the satellite trails and sky region around the trails, respectively.

From Equations (8) through (10), the surface temperature is inversely proportional to the square root of the satellite radius ( $T_{\text{sat}} \propto r_{\text{sat}}^{-1/2}$ ). When assuming the uncertainty  $\delta r_{\text{sat}}$  of 0.5 m, corresponding uncertainty of the surface temperature will be at least  $2 \sim 3$  degrees, which is comparable to the standard deviation of the surface temperature listed in Table 4 ( $\sigma_{T_{\text{sat}}} \sim 2$  K).

#### 4.2.2. Flux model by The Blackbody Radiation

In this section, we model the normalized  $g'$ -,  $R_c$ -, and  $I_c$ -band flux of the Darksat and STARLINK-1113 trails in each epoch with the blackbody radiation. We derived these flux from the normalized and AB magnitudes in

each band (Blanton & Roweis 2007). When modeling the flux of the satellite trails with blackbody radiation, the following four components were considered: thermal radiation of the satellite,  $F_{\text{TS}}$ , reflection of the sunlight,  $F_{\text{RS}}$ , Earthshine,  $F_{\text{REs}}$ , and reflection of Earth thermal radiation,  $F_{\text{TE}}$ . The four components are written as follows (see also Sekiguchi et al. 2003):

$$F_{\text{TS}} = \pi \epsilon \left( \frac{r_{\text{sat}}}{h_{\text{T}}} \right)^2 B(\lambda, T_{\text{sat}}) \frac{\lambda^2}{c}, \quad (12)$$

$$F_{\text{RS}} = \pi \left( \frac{R_{\odot}}{1 \text{ au}} \right)^2 B(\lambda, T_{\odot}) a_{\text{mod}} p(\theta) \left( \frac{r_{\text{sat}}}{h_{\text{T}}} \right)^2 \frac{\lambda^2}{c}, \quad (13)$$

$$F_{\text{REs}} = a_{\text{E}} \left( \frac{R_{\oplus}}{R_{\oplus} + h_{\text{T}}} \right)^2 \left\{ 1 - \left( \frac{R_{\oplus}}{R_{\oplus} + h_{\text{T}}} \right)^2 \right\} \frac{p(\chi)}{p(\theta)} F_{\text{RS}}, \quad (14)$$



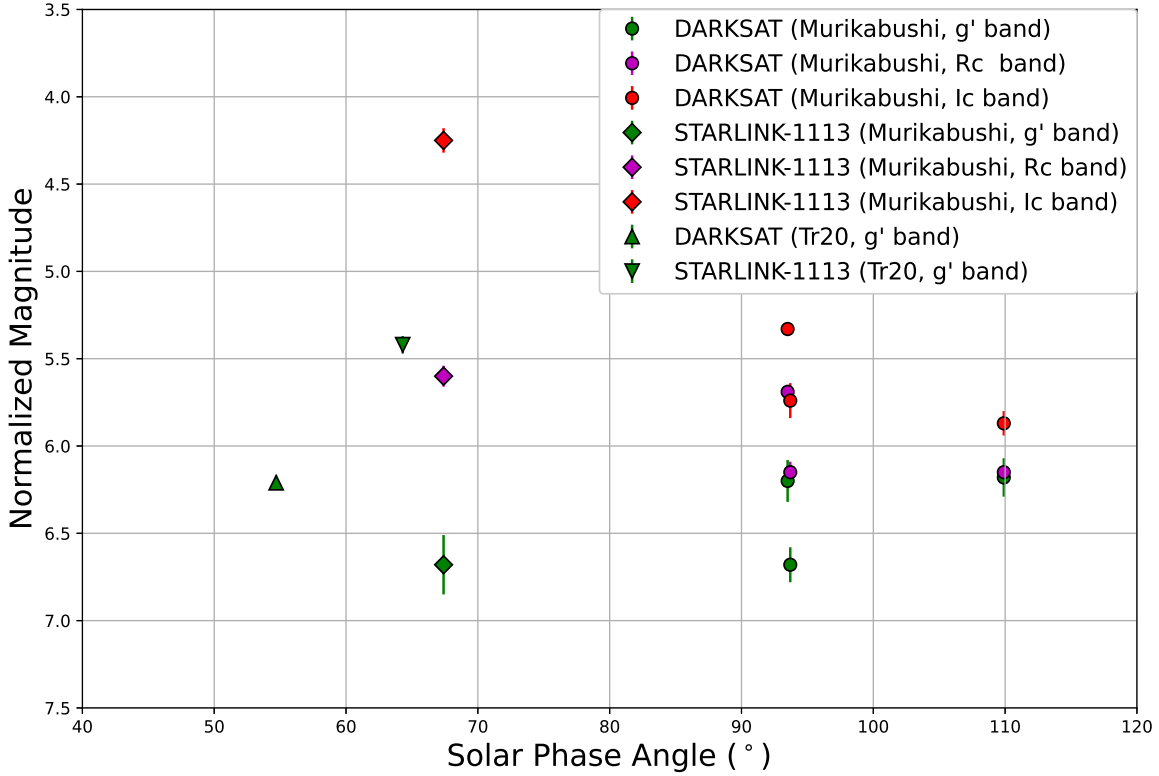


**Figure 6.** A plot between the solar phase angle and normalized  $g'$  (green)-,  $R_c$  (magenta)-, and  $I_c$  (red)-band magnitudes.

$$F_{TE} = \pi \epsilon \left( \frac{R_{\oplus}}{R_{\oplus} + h_T} \right)^2 B(\lambda, T_E) a_{\text{mod}} \left( \frac{r_{\text{sat}}}{h_T} \right)^2 \frac{\lambda^2}{c}, \quad (15)$$

where  $T_{\odot}$  ( $= 5772$  K),  $T_E$  ( $= 290$  K),  $R_{\odot}$  ( $= 7.0 \times 10^5$  km),  $R_{\oplus}$ ,  $h_T$  ( $= 550$  km),  $a_{\text{mod}}$ ,  $a_E$  ( $= 0.3$ ), and  $p(\chi)$  are the temperature of the Sun and the Earth, radius of the Sun and the Earth, orbital height of the LEO satellites, modeled albedo with the blackbody, albedo of the Earth, and phase integral as a function of the Sun-observer-target phase angle  $\chi$ , respectively. The blackbody radiation  $B(\lambda, T)$  is expressed by:

$$B(\lambda, T) = \frac{2hc^2}{\lambda^5} \frac{1}{\exp(\frac{hc}{kT\lambda}) - 1}, \quad (16)$$

where  $c$ ,  $\lambda$ ,  $h$ , and  $k$  are the speed of light, wavelength, the Planck constant, and the Boltzmann constant, respectively. We note that all of the four components (i) are monochromatic flux density per unit frequency, and (ii) are multiplied by a factor,  $(r/h_T)^2$ , for normalization with the orbital height,  $h_T$ . For the derivation of Equations (14) and (15), see Appendix B. The Moon-light effect can be ignored for all three observation epochs, since the Moon was below the horizon at the observa-

tion times (see Appendix C about the Moon effects). In this flux model, we adjusted the albedo of satellite  $a_{\text{mod}}$  with the fixed values of the satellite temperature,  $T_{\text{sat}} = 280$  K, and radius,  $r_{\text{sat}} = 1.5$  m, as explained in the above discussion.

Figure 8 shows the blackbody curves with the flux of the Darksat and STARLINK-1113 trails in Jansky. The flux of Darksat trail is relatively bright in  $g'$  band (April 10, 2020) or comparable in each band (May 18 and June 11, 2020). Meanwhile, the  $g'$ - and  $R_c$ -band flux of STARLINK-1113 are relatively dimmer than that of  $I_c$  band likely due to the strong atmospheric scattering. It is clearly seen that the reflected radiation is dominant in the UV to optical region whereas the thermal radiation is dominant in the mid-infrared region (see also [Hainaut & Williams 2020](#)). By the model fitting with the blackbody radiation, it is confirmed that the modeled albedo of Darksat ( $a_{\text{mod}} = 0.04$ ) is about a half of STARLINK-1113 ( $a_{\text{mod}} = 0.075$ ); these values are consistent with the measured albedo  $a_{\text{obs}}$  in Table 4. Our analysis has demonstrated the effectiveness of the darkening treatment for Darksat. This difference of the

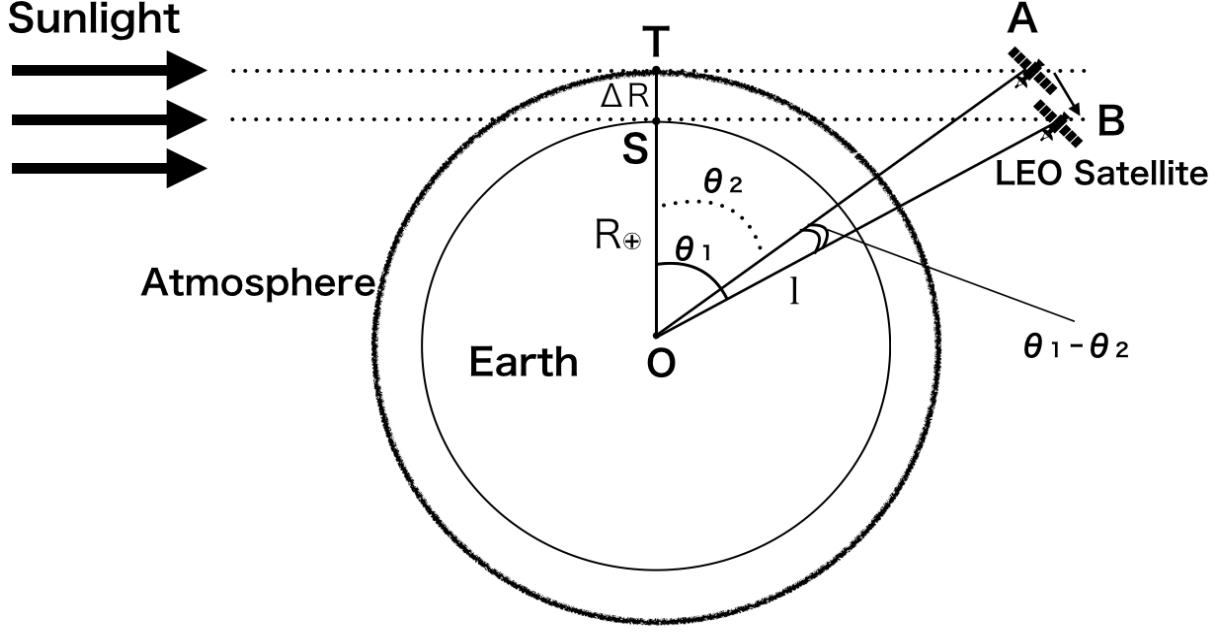


**Figure 7.** The LEO satellite plunging into the Earth shadow (i.e., satellite from point A to B). Points O, S, and T are the geocenter, ground surface, and Kármán line, respectively. The following scales and angles are defined in this figure: the Earth radius,  $R_{\oplus} = |OS| = 6,371$  km, atmospheric thickness,  $\Delta R = |ST| = 100$  km, orbital height from the geocenter,  $l = |OA| = |OB| = 6,921$  km,  $\theta_1$  ( $\angle BOS$ ), and  $\theta_2$  ( $\angle AOT$ ). The LEO satellite orbits the region formed by  $\angle BOA$  ( $\theta_1 - \theta_2$ ) where the Sunlight to the satellite is strongly affected by the Earth’s atmosphere.

satellite-surface albedo corresponds to Darksat being  $\sim 0.75$  mag darker than STARLINK-1113; this magnitude difference between the two satellites is consistent with the result of Tr20. Since it was difficult to fit the  $g'$ -band flux with the single-albedo blackbody model, the difference between  $g'$ -band flux and that of the other bands probably reflects the physical properties of the surface of these satellites.

## 5. CONCLUSIONS

Using the 105 cm Murikabushi telescope with *MITSuME* system, we conducted the simultaneous multicolor ( $g'$ ,  $R_c$ , and  $I_c$  bands) observations for the Starlink’s LEO satellites Darksat and STARLINK-1113 on April 10, May 18, and June 11, 2020. Our observational results are summarized as follows:

- (1) The apparent  $g'$ -band magnitudes of Darksat are comparable to or brighter than that of STARLINK-1113;
- (2) The shorter the observed wavelength is, the fainter satellite magnitudes tend to become;
- (3) At the vicinity of the Earth shadow, the reflected flux by STARLINK-1113 is extremely ( $> 1.0$  mag) redder than that of Darksat, excluding the difference of  $g' - R_c$ ;

- (4) There is no correlation between the solar phase angle and orbital-altitude-scaled magnitude; and
- (5) The flux-model fitting to the satellite trails by the blackbody radiation resulted in that the albedo of Darksat is about a half of STARLINK-1113.

The result (1) is contrary to that of Tr20. However, our results could be explained by taking into account both the solar and observer phase angles and atmospheric extinction qualitatively.

In June 3, 2020, Space X newly launched its eighth batch of Starlink’s LEO satellites<sup>7</sup>. These satellites include STARLINK-1436 (nicknamed “Visorsat”) with a deployable Sun visor to prevent sunlight and reduce reflected flux. Henceforth, it is important to compare the astronomical impacts of the usual Starlink’s LEO satellites, Darksat, and Visorsat. For precise verification of solar and observer phase angle dependence of satellite magnitudes, it is needed to carry out multicolor-multispot observation for the Starlink’s LEO satellites including Darksat and Visorsat.

<sup>7</sup> <https://www.spaceflightinsider.com/missions/starlink/first-starlink-visorsat-takes-flight-aboard-spacex-falcon-9/>



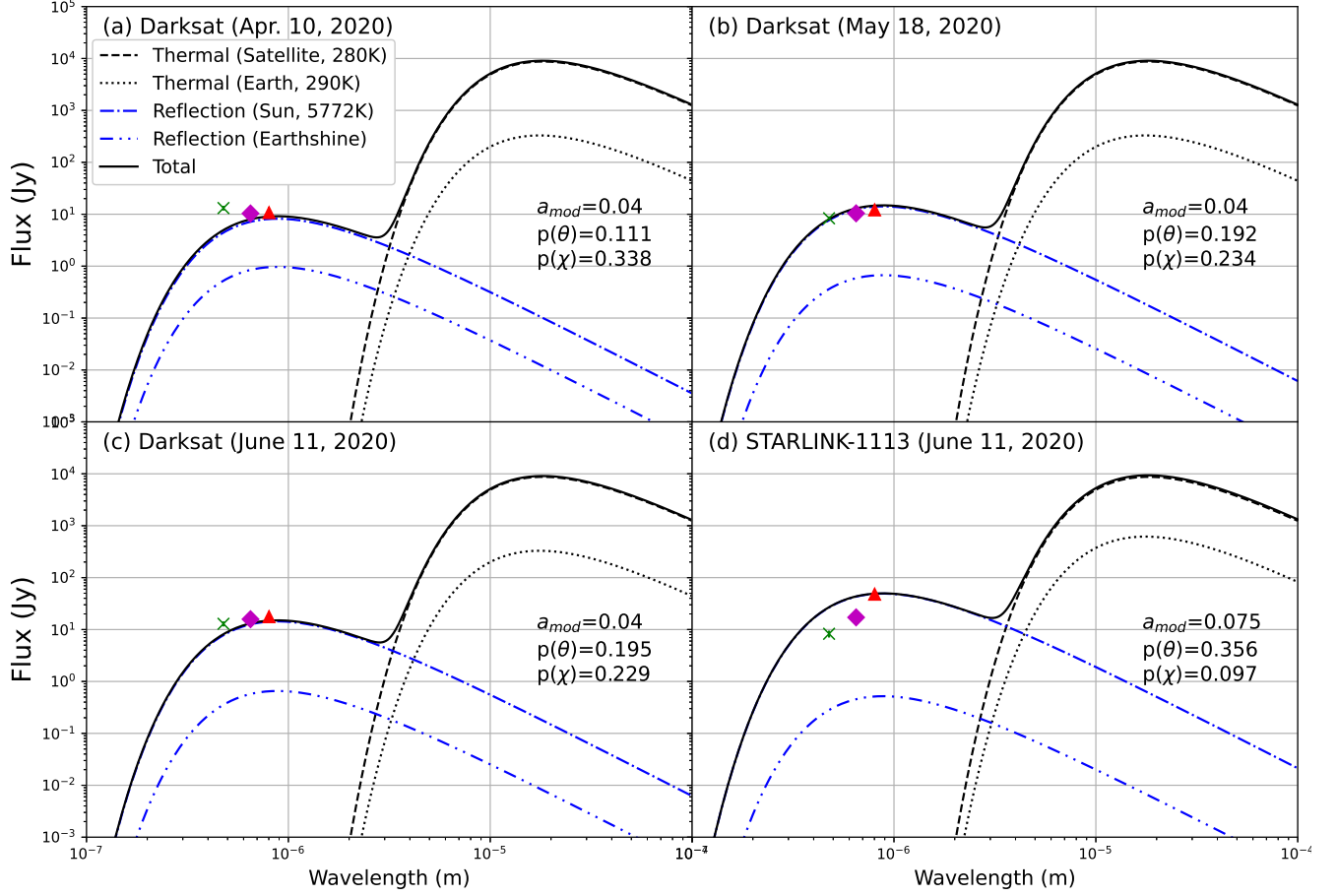


**Figure 8.** Modeling the  $g'$ - (green),  $R_c$ - (magenta), and  $I_c$  (red)-band AB flux of Darksat (panels a, b, and c) and STARLINK-1113 (panel d) by the black-body radiation. In each band, the x-axis values of AB flux data points correspond to the effective wavelengths (see Section 2). Blue dash-dot, chain double-dashed, black dotted, dashed, and solid lines imply the reflection of the Sunlight, Earthshine, reflection of the Earth-thermal radiation, thermal radiation from these satellites, and total flux, respectively. The albedo,  $a_{mod}$ , phase angle,  $p(\theta)$ , and  $p(\chi)$  are described in each panel.

#### ACKNOWLEDGMENTS

We are grateful to the staff in IAO and Yaeyama Star Club for supporting the authors (TH and HH) while preparing the paper. MO is also grateful to all the staff of the Public Relations Center, NAOJ. We appreciate the reviewer for his/her valuable comments for improving this paper. The fourth U.S. Naval Observatory CCD Astrograph Catalog (UCAC4) is provided by Zacharias N., Finch C.T., Girard T.M., Henden A., Bartlet J.L., Monet D.G., Zacharias M.I. The MITSuME system was supported by a Grant-in-Aid for Scientific Research on Priority Areas (19047003).

#### REFERENCES

- |  |   |
|--|---|
| Blanton, M. R., & Roweis, S. 2007, AJ, 133, 734        | Jordi, K., Grebel, E. K., & Ammon, K. 2006, A&A, 460, |
| Hainaut, O. R., & Williams, A. P. 2020, A&A, 636, A121 | 339   |

**Table 1.** Observation log of Darksat and STARLINK-1113 by the Murikabushi telescope/*MITSuME*  $g'$ ,  $R_c$  and  $I_c$  bands

	Darksat	Darksat	Darksat	STARLINK-1113
Observation Date	April 10, 2020	May 18, 2020	June 11, 2020	June 11, 2020
Start Time of Observation (UTC)	10:53:50	11:13:55	12:31:56	12:17:56
Central Time of Observation (UTC)	10:54:00	11:14:00	12:31:58.5	12:17:58.5
End Time of Observation (UTC)	10:54:10	11:14:05	12:32:01	12:18:01
Exposure Time (s)	20.0	10.0	5.0	5.0
RA <sup>a</sup>	05:52:35.05	09:04:46.3	10:42:36.7	12:23:17.5
Dec <sup>a</sup>	-05:18:43.8	-13:58:57.0	-13:34:37.2	-25:03:20.0
Azimuth <sup>a, b</sup> (°)	236.67	223.29	238.57	205.66
Elevation <sup>a</sup> (°)	42.49	40.00	26.96	35.80
Airmass <sup>a</sup>	1.48	1.55	2.20	1.71
Altitude <sup>a</sup> (km)	550.16	549.88	549.72	549.56
Distance between Satellite and Observer (km)	781.54 ± 3.12	812.03 ± 25.62	1068.69 ± 0.91	873.41 ± 6.36
Solar Phase Angle <sup>a</sup> [Sun-Target-Observer] (°)	109.9	93.7	93.5	67.4
Phase Angle <sup>a</sup> [Sun-Observer-Target] (°)	70.1	86.3	86.5	112.6
Observer Phase Angle <sup>a</sup> (°)	42.9	44.8	55.1	48.3
Angular Velocity (arcsec s <sup>-1</sup> )	1934.10 ± 10.88	1322.99 ± 76.20	1415.33 ± 2.35	1626 ± 22.03

<sup>a</sup>Values at the central time of observations.<sup>b</sup>The north and the east are 0° and 90°, respectively.



- Lebofsky, L. A., Sykes, M. V., Tedesco, E. F., et al. 1986, *Icarus*, 68, 239
- Mallama, A. 2020, arXiv:2003.07805
- McDowell, J. C. 2020, *ApJL*, 892, L36
- Minnaert, M. 1941, *ApJ*, 93, 403
- Sekiguchi T., Abe M., Boehnhardt H., et al., 2003, *A&A*397, 325
- Spencer, J. R., Lebofsky, L. A., & Sykes, M. V. 1989, *Icarus*, 78, 337
- Stamnes, K., Thomas, G. E., & Stamnes, J. J. 1999, *Radiative Transfer in the Atmosphere and Ocean*, 2nd edn. (Cambridge University Press)
- Tregloan-Reed, J., Otarola, A., Ortiz, E., et al. 2020 (Tr20), *A&A*, 637, L1
- Tyson, J. A., Ivezić, Ž., Bradshaw, A., et al. 2020, arXiv e-prints, arXiv:2006.12417
- Whitmell, C. T. 1907, *The Observatory*, 30, 96
- Willmer, C. N. A. 2018, *ApJS*, 236, 47

**Table 2.** Magnitudes of Darksat, STARLINK-1113, and reference stars

Reference Star	$g'$ magnitude <sup>a</sup> (Star)	$g'$ magnitude (Satellite)	$R_c$ magnitude <sup>a</sup> (Star)	$R_c$ magnitude (Satellite)	$I_c$ magnitude <sup>a</sup> (Star)	$I_c$ magnitude (Satellite)
Date: April 10, 2020, Target: Darksat						
UCAC4 424-011322	12.53	$6.98 \pm 0.11$	10.68	$6.92 \pm 0.04$	9.75	$6.62 \pm 0.07$
UCAC4 424-011295	12.41	$6.91 \pm 0.11$	10.93	$6.91 \pm 0.04$	10.16	$6.65 \pm 0.07$
Apparent Magnitude <sup>b</sup>	...	$6.95 \pm 0.11$	...	$6.92 \pm 0.04$	...	$6.64 \pm 0.07$
Normalized Magnitude	...	$6.18 \pm 0.11$	...	$6.15 \pm 0.04$	...	$5.87 \pm 0.07$
Date: May 18, 2020, Target: Darksat						
BD-13 2755	10.89	$7.66 \pm 0.07$	10.05	$7.03 \pm 0.06$	9.59	$6.58 \pm 0.07$
TYC 5457-786-1	12.32	$7.39 \pm 0.07$	11.77	$6.96 \pm 0.06$	11.38	$6.59 \pm 0.08$
Apparent Magnitude <sup>b</sup>	...	$7.52 \pm 0.07$	...	$6.99 \pm 0.06$	...	$6.59 \pm 0.07$
Normalized Magnitude	...	$6.68 \pm 0.10$	...	$6.15 \pm 0.09$	...	$5.74 \pm 0.10$
Date: June 11, 2020, Target: Darksat						
TYC 5498-663-1	11.33	$7.76 \pm 0.04$	10.77	$7.15 \pm 0.03$	10.45	$6.71 \pm 0.02$
TYC 5498-1307-1	12.54	$7.53 \pm 0.16$	12.03	$7.12 \pm 0.04$	11.69	$6.83 \pm 0.05$
Apparent Magnitude <sup>b</sup>	...	$7.65 \pm 0.12$	...	$7.13 \pm 0.04$	...	$6.77 \pm 0.04$
Normalized Magnitude	...	$6.20 \pm 0.12$	...	$5.69 \pm 0.04$	...	$5.33 \pm 0.04$
Average value of the three epochs						
Apparent Magnitude <sup>b</sup>	...	$7.37 \pm 0.10$	...	$7.01 \pm 0.05$	...	$6.66 \pm 0.06$
Normalized Magnitude	...	$6.35 \pm 0.10$	...	$6.00 \pm 0.06$	...	$5.65 \pm 0.08$
Date: June 11, 2020, Target: STARLINK-1113						
UCAC4 325-067504	13.76	$7.59 \pm 0.23$	12.44	$6.59 \pm 0.05$	11.72	$5.12 \pm 0.07$
UCAC4 325-067505	13.18	$7.48 \pm 0.16$	12.61	$6.62 \pm 0.10$	12.17	$5.10 \pm 0.10$
CD-24 10321	10.42	$8.00 \pm 0.04$	9.37	$6.62 \pm 0.02$	8.66	$5.53 \pm 0.02$
Apparent Magnitude <sup>b</sup>	...	$7.69 \pm 0.16$	...	$6.61 \pm 0.06$	...	$5.25 \pm 0.07$
Normalized Magnitude	...	$6.68 \pm 0.17$	...	$5.60 \pm 0.06$	...	$4.25 \pm 0.07$

<sup>a</sup>Converted UCAC4 magnitudes by Equations (3), (4), and (5).

<sup>b</sup>Averaged magnitude with the above reference stars.

**Table 3.** Colors of Darksat and STARLINK-1113

Target Satellite	Date	$g' - R_c$	$g' - I_c$	$R_c - I_c$
Darksat	April 10, 2020	$0.03 \pm 0.12$	$0.31 \pm 0.13$	$0.28 \pm 0.08$
Darksat	May 18, 2020	$0.53 \pm 0.09$	$0.93 \pm 0.10$	$0.41 \pm 0.10$
Darksat	June 11, 2020	$0.51 \pm 0.13$	$0.87 \pm 0.13$	$0.36 \pm 0.05$
Average	...	$0.36 \pm 0.11$	$0.71 \pm 0.12$	$0.35 \pm 0.08$
STARLINK-1113	June 11, 2020	$1.08 \pm 0.18$	$2.44 \pm 0.18$	$1.36 \pm 0.09$



**Table 4.** The phase integral, absolute magnitude, measured albedo, and surface temperature of Darksat and STARLINK-1113

Target Satellite (Filter, Date)	Phase Integral $p(\theta)$	Absolute Magnitude $H^a$	Albedo $a_{\text{obs}}^a$	Temperature $T_{\text{sat}}^a$ (K)
Darksat ( $g'$ -band, April 10, 2020)	0.11	30.97	0.12	277.38
Darksat ( $g'$ -band, May 18, 2020)	0.19	32.05	0.04	283.04
Darksat ( $g'$ -band, June 11, 2020)	0.19	31.59	0.07	281.31
Darksat ( $R_c$ -band, April 10, 2020)	0.11	30.94	0.06	282.01
Darksat ( $R_c$ -band, May 18, 2020)	0.19	31.52	0.03	283.77
Darksat ( $R_c$ -band, June 11, 2020)	0.19	31.07	0.05	282.49
Darksat ( $I_c$ -band, April 10, 2020)	0.11	30.66	0.06	282.17
Darksat ( $I_c$ -band, May 18, 2020)	0.19	31.12	0.04	283.58
Darksat ( $I_c$ -band, June 11, 2020)	0.19	31.71	0.05	282.34
Averaged Temperature	...	...	...	282.01
STARLINK-1113 ( $g'$ -band, June 11, 2020)	0.36	32.73	0.02	284.55
STARLINK-1113 ( $R_c$ -band, June 11, 2020)	0.36	31.66	0.03	284.06
STARLINK-1113 ( $I_c$ -band, June 11, 2020)	0.36	30.30	0.08	280.49
Averaged Temperature	...	...	...	283.07

<sup>a</sup>The radius of the satellites,  $r_{\text{sat}}$ , is fixed to 1.5 m.

## APPENDIX

## A. APPROXIMATE BRDF MODEL

Contrary to the results of Tr20, the apparent and normalized magnitudes of STARLINK-1113 are fainter than or comparable to those of Darksat except for the  $I_c$ -band magnitude (Figure 6). Here, we examine both the solar and observer phase-angle effects of Darksat and STARLINK-1113. The definition of the observer phase angle is the angle between the straight line from the geocenter to the satellite and the straight line from the observer to the satellite (see the angle  $c$  in Figure 1 of [Mallama 2020](#)). The previous study, Tr20, estimated a parametrised bidirectional reflectance distribution function (BRDF) model by [Minnaert \(1941\)](#) to investigate the two phase-angle effects approximately. They evaluated the ratio,  $R$ , which is the index of solar phase attenuation between the two satellites:

$$R = \left( \frac{\cos \theta_{1113} \cos \phi_{1113}}{\cos \theta_{DS} \cos \phi_{DS}} \right)^{1-k}, \quad (\text{A1})$$

where  $\theta_{DS}$  (or  $\theta_{1113}$ ) and  $\phi_{DS}$  (or  $\phi_{1113}$ ) are the solar and observer phase angle of Darksat (or STARLINK-1113), respectively. The Minnaert exponent  $k$  ranges from 0 to 1. If the ratio  $R$  is  $> 1$  (or  $< 1$ ), a phase-angle-dependent reflectance of Darksat (or STARLINK-1113) is dominant. Figure A shows the ratio  $R(k)$  as a function of the Minnaert exponent  $k$  on June 11, 2020 with the  $R(k)$  in Tr20. In this study, the phase angle component of reflected flux of Darksat is dominant for any  $k$ . Tr20 assumed a dark surface ( $k = 0.5$ ; [Stamnes et al. 1999](#)) for Darksat and STARLINK-1113. When  $k = 0.5$ ,  $R(k)$  in this study will be  $\sim 0.68$  corresponding to 0.42 mag darkening of Darksat relative to STARLINK-1113. Since the normalized  $g'$ - (or  $R_c$ -) band magnitude of Darksat on June 11, 2020 (third data points from the right in Figure 6) is already brighter than (or comparable to) that of STARLINK-1113, the correction by BRDF (i.e., brighten the Darksat magnitude by 0.42 mag) leads the result that STARLINK-1113 is always darker than Darksat in  $g'$  and  $R_c$  band.

## B. REFLECTION OF THE EARTHLIGHT AND EARTH THERMAL RADIATION

This chapter describes the derivation for the reflection flux of the earthlight,  $F_{REs}$ , and Earth thermal radiation,  $F_{TE}$ , from the LEO satellite to an observer. The definition of the following parameters is the same as defined in Section 4.

## B.1. Reflection of The Earthlight

The thermal radiation density of the Sun received by the Earth,  $F_{SE}$ , is expressed by:

$$\begin{aligned} F_{SE} &= 4\pi B(\lambda, T_{\odot}) \frac{\pi R_{\odot}^2}{4\pi (1 \text{ au})^2} \frac{\lambda^2}{c} \\ &= \pi \left( \frac{R_{\odot}}{1 \text{ au}} \right)^2 B(\lambda, T_{\odot}) \frac{\lambda^2}{c}, \end{aligned} \quad (\text{B1})$$

$$B(\lambda, T) = \frac{2hc^2}{\lambda^5} \frac{1}{\exp\left(\frac{hc}{kT\lambda}\right) - 1}. \quad (\text{B2})$$

As shown in Figure B, considering the distance from the Earth surface and the cross-sectional area of the Earth with respect to the cross-sectional area limited by the sphere with radius  $l$  centered at the LEO satellite, the flux of the earthlight received by the LEO satellite,  $F_{ER,sat}$ , is written as follows:

$$\begin{aligned} F_{ER,sat} &= a_E F_{SE} \frac{\pi (R_{\oplus} \sin \theta_E)^2}{\pi R_{\oplus}^2} \times \frac{R_{\oplus}^2}{(R_{\oplus} + h_T)^2} \\ &= a_E F_{SE} \left( \frac{R_{\oplus}}{R_{\oplus} + h_T} \right)^2 \left\{ 1 - \left( \frac{R_{\oplus}}{R_{\oplus} + h_T} \right)^2 \right\}, \end{aligned} \quad (\text{B3})$$

where  $\theta_E$  is the angle between the line from the geocenter to the LEO satellite and the line from the geocenter to the interacting point on the ground surface with the tangent line between the LEO satellite and ground surface. As a result, the earthlight flux from the LEO satellite received by an observer,  $F_{REs}$ , is described by:

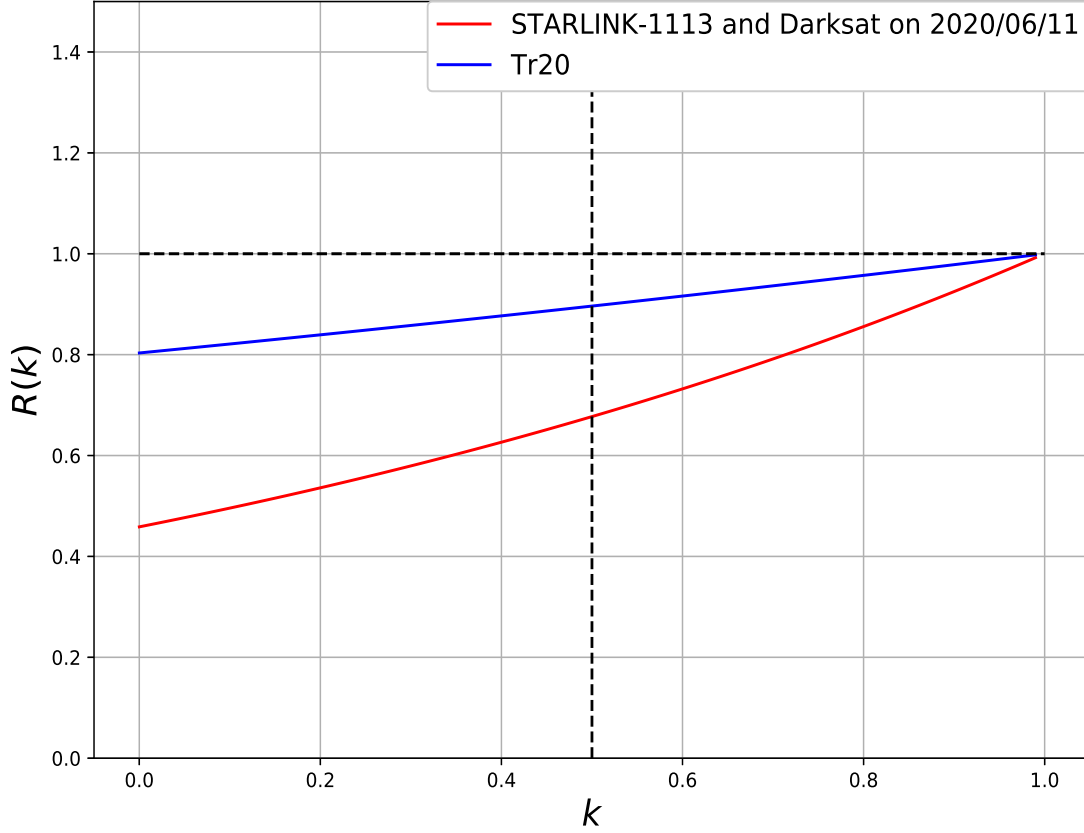


**Figure A.** The ratio  $R(k)$  in each epoch with the result of Tr20. The horizontal and vertical dashed lines imply an auxiliary line of  $R(k) = 1$  and the Minnaert exponent  $k$  of 0.5 (i.e., for a dark surface), respectively.

$$\begin{aligned}
 F_{\text{REs}} &= F_{\text{ER,sat}} a_{\text{mod}} \left( \frac{r_{\text{sat}}}{r} \right)^2 p(\chi) \left( \frac{r}{h_{\text{T}}} \right)^2 \\
 &= \pi \left( \frac{R_{\odot}}{1 \text{ au}} \right)^2 B(\lambda, T_{\odot}) a_{\text{E}} \left( \frac{R_{\oplus}}{R_{\oplus} + h_{\text{T}}} \right)^2 \left\{ 1 - \left( \frac{R_{\oplus}}{R_{\oplus} + h_{\text{T}}} \right)^2 \right\} a_{\text{mod}} \left( \frac{r_{\text{sat}}}{h_{\text{T}}} \right)^2 p(\chi) \frac{\lambda^2}{c} \\
 &= a_{\text{E}} \left( \frac{R_{\oplus}}{R_{\oplus} + h_{\text{T}}} \right)^2 \left\{ 1 - \left( \frac{R_{\oplus}}{R_{\oplus} + h_{\text{T}}} \right)^2 \right\} \frac{p(\chi)}{p(\theta)} F_{\text{RS}},
 \end{aligned} \tag{B4}$$

where this flux is normalized with the orbital height,  $h_{\text{T}}$ , by the factor,  $(r/h_{\text{T}})^2$ .

### B.2. Reflection of The Earth thermal radiation

The thermal radiation density of the Earth received by the LEO satellite,  $F_{\text{ET,sat}}$ , is evaluated as follows:

$$\begin{aligned}
 F_{\text{ET,sat}} &= 4\pi\epsilon B(\lambda, T_{\text{E}}) \frac{\pi(R_{\oplus} \sin \theta_{\text{E}})^2}{4\pi l^2} \frac{\lambda^2}{c} \\
 &= \pi\epsilon \left( \frac{R_{\oplus}}{R_{\oplus} + h_{\text{T}}} \right)^2 B(\lambda, T_{\text{E}}) \frac{\lambda^2}{c}.
 \end{aligned} \tag{B5}$$



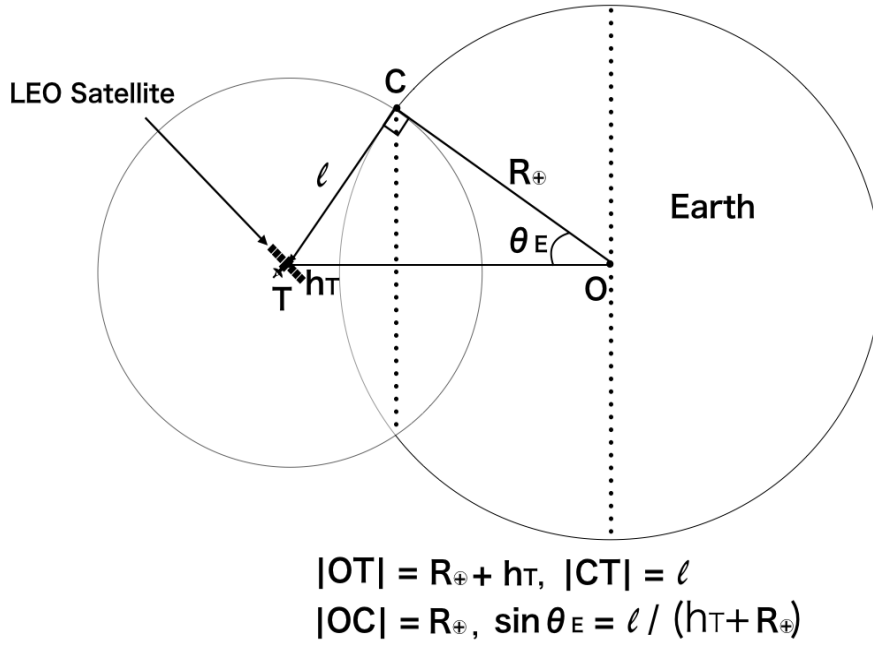


**Figure B.** The cross-sectional area of the Earth with respect to the cross-sectional area limited by the sphere centered at the LEO satellite. Where  $\theta_E$  is the angle between the line from the geocenter (Point O) to the the LEO satellite (Point T) and the line from the geocenter to the interacting point on the ground surface with the tangent line (length  $\ell$ ) between the LEO satellite and ground surface (Point C).

Namely, the Earth thermal radiation from the LEO satellite received by an observer,  $F_{TE}$ , normalized with the orbital height is expressed by:

$$\begin{aligned}
 F_{TE} &= F_{ET, \text{sat}} a_{\text{mod}} \left( \frac{r}{h_T} \right)^2 \\
 &= \pi \epsilon \left( \frac{R_{\oplus}}{R_{\oplus} + h_T} \right)^2 B(\lambda, T_E) a_{\text{mod}} \left( \frac{r_{\text{sat}}}{h_T} \right)^2 \frac{\lambda^2}{c}.
 \end{aligned} \tag{B6}$$

### C. THERMAL- AND REFLECTED-SATELLITE FLUX BY THE MOON

In Section 4, we discussed the normalized thermal and reflected flux of Darksat and STARLINK-1113 without the effect by the Moon. The normalized thermal,  $F_{TM}$ , and reflected flux,  $F_{RM}$ , of the satellites by the Moon are described with:

$$F_{TM} = \pi \epsilon \left( \frac{R_{\text{Moon}}}{D_{\text{Moon}}} \right)^2 B(\lambda, T_{\text{Moon}}) a p(\theta) \left( \frac{r_{\text{sat}}}{h_T} \right)^2 \frac{\lambda^2}{c}, \tag{C1}$$

$$F_{RM} = \pi \left( \frac{R_{\odot}}{1 \text{ au}} \right)^2 B(\lambda, T_{\odot}) a_{\text{Moon}} p(\theta_{\text{Moon}}) \left( \frac{R_{\text{Moon}}}{D_{\text{Moon}}} \right)^2 a p(\theta) \left( \frac{r_{\text{sat}}}{h_T} \right)^2 \frac{\lambda^2}{c}, \tag{C2}$$

where  $R_{\text{Moon}} (= 1.73 \times 10^3 \text{ km})$ ,  $T_{\text{Moon}}$ ,  $a_{\text{Moon}} (= 0.12)$ ,  $\theta_{\text{Moon}}$  (or  $\theta$ ),  $p(\theta_{\text{Moon}})$  (or  $p(\theta)$ ), and  $D_{\text{Moon}} (= 3.83 \times 10^5 \text{ km})$  are the Moon radius, irradiated-Moon-surface temperature, albedo of the Moon, Sun-Moon-satellite (or Moon-satellite-observer) phase angle, phase integral, and the distance between an observer and the Moon, respectively. The definition of the other parameters in Equations (C1) and (C2) is the same as defined in Section 4.